Laser-Assisted Gas Metal Arc Welding of 25-mm-Thick HY-80 Plate

Toughness properties were evaluated with dynamic tear and explosion bulge testing

BY C. V. HYATT, K. H. MAGEE, J. F. PORTER, V. E. MERCHANT AND J. R. MATTHEWS

ABSTRACT. Laser-assisted gas metal arc welding of HY-80 steel was investigated. The effect of welding parameters was studied and optimum welding conditions were identified. Welding using Lincoln LA-100 wire on 25-mm-thick HY-80 plate with a four-pass technique, a double 45-deg groove preparation, 9.5 mm deep with no root opening, a heat input of 1.6 kJ/mm and a 50% Ar-50% He gas shield produced a predominately martensitic weld metal microstructure. An acicular ferrite weld metal microstructure could not be produced for any set of processing conditions investigated. This is believed to be a result of the high levels of dilution. The toughness of the laser-assisted gas metal arc welds was assessed with dynamic tear testing and explosion bulge testing. Toughness was found to be low but highly variable. Optimum electrode chemistry would probably allow the toughness to be improved.

Introduction

Laser-assisted gas metal arc welding (LAGMAW) is a hybrid process that combines energy from a laser with energy from a gas metal arc welding process. Based on previous experiments with mild steel (Refs. 1, 2), combining arc energy with a 5-kW laser, the process has the potential to achieve weld penetration equivalent to that of a 20- to 25-kW laser. With the hybrid process, the small heat-affected zone and low distortion typical of laser welding are largely retained. This is because, in addition to directly heating the weldment, the laser acts to focus the arc by heating its path through it. This increases arc conductivity along the path of the laser beam, and, thus, more arc energy flows along the higher conductivity path (Refs. 1–4).

This study addresses the question of whether laser-assisted gas metal arc welding is a promising technique for the welding of HY-80 steel. The characteristics of materials and equipment used are reported first. Experiments to establish optimum welding conditions and understand variables that influence weldment characteristics are reported next. The effect of welding conditions on the microstructure of HY-80 steel weldments are then reported, along with the conditions selected to prepare plates from which dynamic tear and explosion bulge specimens were removed. This is followed with data on the toughness of these HY-80 weldments. Finally, comments are made on the performance of this welding method relative to others and on what needs to be done if this technique is to become viable in engineering practice.

Materials

CSA grade 40.21 300W steel was used during the initial phases of the investigation aimed at quantifying the effect of various process parameters on the weld pool's physical dimensions. Trials were subsequently performed on HY-80 steel plate to develop a processing procedure that produced acceptable weld and heat-affected zone microstructures. The compositions of these materials are shown in Table 1. All trials were performed on coupons measuring approximately 50 mm x 102 mm x plate thickness, which were ground to remove mill scale from the weld region, and degreased immediately prior to welding. Weldments were produced using 1.6-mm-diameter Lincoln LA-100 wire, the composition of which is also shown in Table 1.

KEY WORDS

Laser Assist
Gas Metal Arc
Low Distortion
Lasers
HY-80 Plate
Joint Penetration

Equipment

Trials were performed using a Combustion Engineering Industrial CE 5000 carbon dioxide laser, with a rated continuous wave output of 5.5 kW. The laser light was directed to the workpiece via a 38-cm focal length, antireflection coated zinc selenide lens, or a 50.8-mm concave molybdenum alloy mirror. In either case, the beam was focused to a spot size of approximately 1-mm diameter.

A Hobart Mega-Flux 450-RV5 constant voltage/constant current power supply with a rated output of 450 A, 38 V DC at 100% duty cycle was used for the gas metal arc welding. All LAGMAW trials were conducted using the power source in a DC-electrode-positive, constant-voltage configuration. The welding current was varied by changing the electrode wire feed rate.

A CNC 5-axis workstation capable of providing linear movement of up to 169 mm/s was used to achieve the desired range of welding speeds. A gas-shielding device designed to provide an inert gas blanket to the area surrounding the weld

C. V. HYATT, J. F. PORTER AND J. R. MATTHEWS are with Defence Research Establishment Atlantic, Nova Scotia, Canada. K. H. MAGEE is with Canspec Group, Inc., and V. E. MERCHANT is with Convergent Prima, Inc.

Table 1 — Chemical Composition of the Steel Plates and the Lincoln LA-100 Electrode Wire

Steel	C	Mn	Si	S	P	Ni	Cr	Mo	Cu	V	Al	Ti
HY80	0.13	0.29	0.20	<0.006	0.006	2.42	1.49	0.41	0.08	<0.01	—	<0.02
300W	0.18	1.23	0.18	0.008	0.019	—	—	—	—	0.05	0.04	—
Wire	0.06	1.55	0.37	0.015	0.012	1.80	0.05	0.33	0.07	<0.02	0.02	0.01

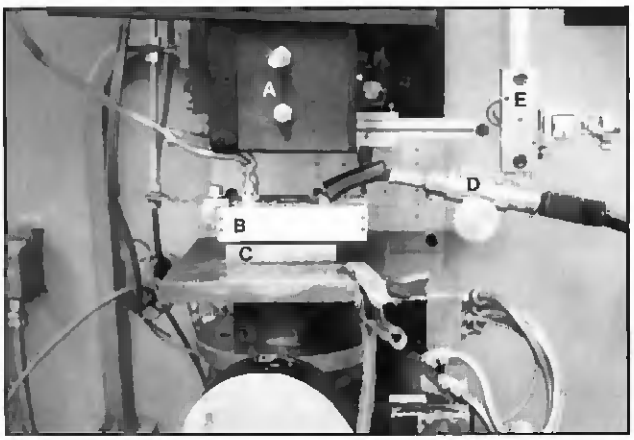

Fig. 1 — Experimental set up. A — Laser focusing optics head; B — gas shield; C — coupon; D — GMAW gun; E — rack boxes and arms.

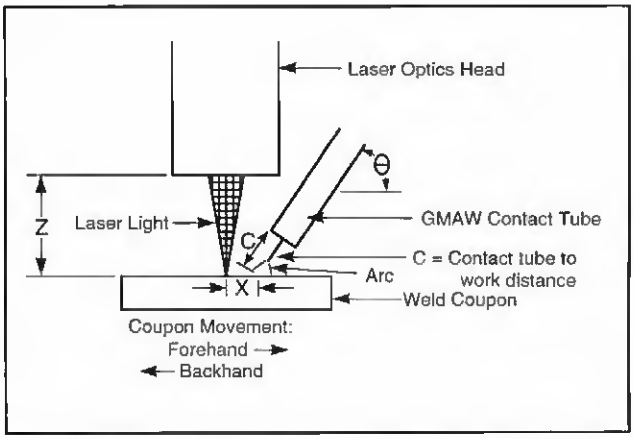

Fig. 2 — GMAW gun and laser optics head positioning parameters.

Table 2 — Basic LAGMAW Operating Parameters

Electrode angle, θ	50 deg
Contact-tube-to-work distance, C	15.2 mm
Laser head assembly to coupon, Z	152 mm
Laser spot to electrode, X	0 mm
Shielding gas composition	helium
Electrode wire diameter	1.6 mm

Table 3 — Bead-on-Plate LAGMAW Weld Pool Dimensions for Helium-Argon Shielding Gases

Gas Composition	Weld Depth (mm)	Weld Width (mm)	Aspect Ratio
100% He	9.8	11.4	0.85
75% He–25% Ar	9.5	11.8	0.80
50% He–50% Ar	9.5	12.4	0.176
100% Ar	7.5	14.1	0.53

pool was fabricated. This device was not used for all the trials as the gas shield provided by the GMAW gun proved adequate for preventing atmospheric contamination. Manual positioning of the GMAW gun was achieved using commercially available rack arms and boxes. The experimental setup is shown in Fig. 1.

In some cases, especially for preliminary trials, small coupons about 25 cm long by 5 cm wide were used. To ensure the small coupon size did not have an influence on microstructural development, a coupon holder, which simulated the heat flow in larger pieces and prevented distortion, was used. Details of the device are given elsewhere (Ref. 5).

Determination of LAGMAW Operating Parameters

A number of trials were done to optimize and understand the operating parameters of the LAGMAW process. The parameters considered included laser power and focus, arc current and voltage, gas shield and the system geometric factors shown in Fig. 2. These geometric factors included the torch angle, the contact-tube-to-work distance, the position of the wire tip with respect to the laser spot and the vertical distance of the laser optics head. In most cases, forehand welding and bead-on plate techniques were used. As a starting point the conditions listed in Table 2, which had been reported in an earlier study (Ref. 1), were used.

Geometric Factors

The effect of gun angle, contact-tube-to-work distance and current are well-known characteristics of the GMAW process. For the hybrid process, to ensure the arc and laser energies were directed to the same location on the workpiece, alignment of the laser spot and the electrode tip was also important. Inconsistent penetration was observed when the laser spot was positioned behind the GMAW weld pool, probably because the laser light hit the electrode rather than the melt pool produced by the welding arc. Increasing the GMAW voltage was found to produce a negligible effect on penetration, but produced wider weld beads. Finally, trials revealed the optimum penetration could be achieved when the focal point of the laser light beam was positioned slightly further below the top of the workpiece (approximately 0.7 mm) than was required to produce maximum penetration during laser welding alone. This shift in the point of focus has been observed previously and is attributable to a depression of the weld pool surface by the welding arc (Ref. 2).

Laser Energy

The introduction of laser energy into the GMAW process was shown to have a greater influence on the depth of penetration at lower arc welding currents — Fig. 3. This effect may be the result of the laser light being partially absorbed or deflected by the additional arc plasma generated at higher current levels. The maximum current was generally limited to approximately 450 A using a 1.6-mm-

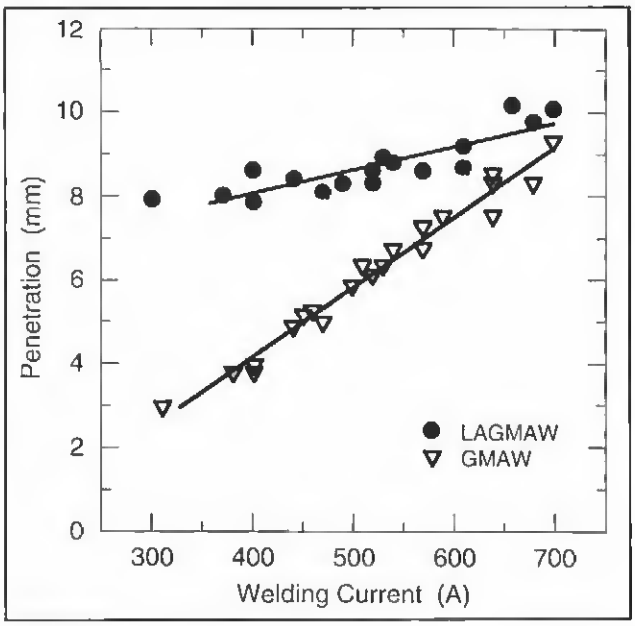

Fig. 3 — Comparison of LAGMAW and GMAW penetration (1.59-mm electrode, 16.9-mm/s travel speed, 5.7-kW laser output power).

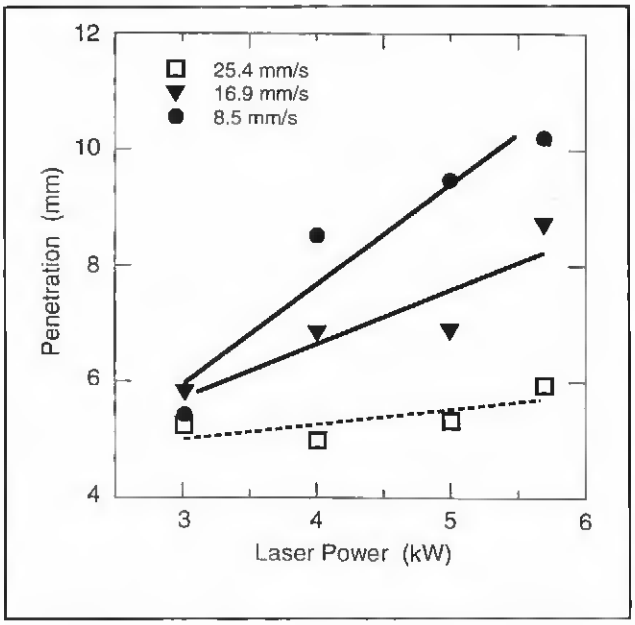

Fig. 4 — LAGMAW penetration as a function of travel speed and laser power (1.14-mm electrode, 35 V, 350–370 A).

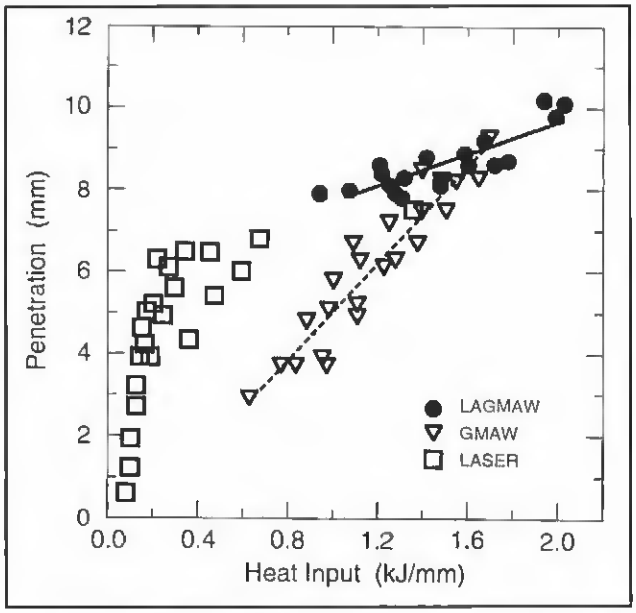

Fig. 5 — Effect of heat input on penetration achieved in LAGMA GMA and laser welds.

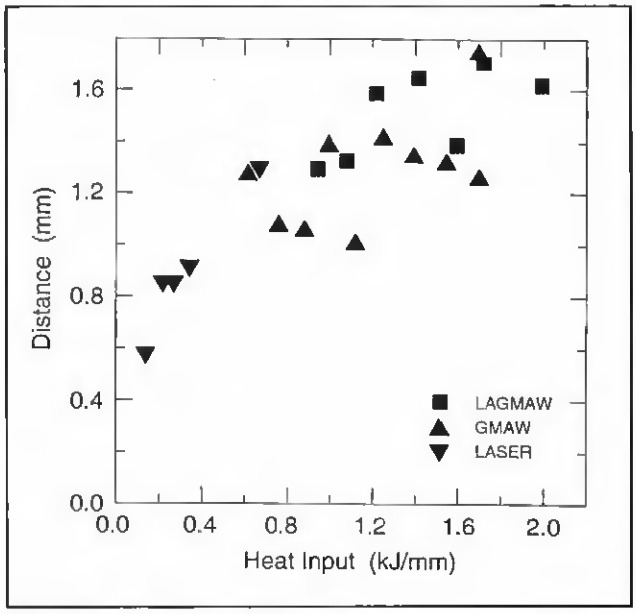

Fig. 6 — Effect of heat input on the heat-affected zone width measured from the weld interface of the coupon.

diameter wire due to the generally poor bead profile obtained at higher current levels. The effect of laser power output was found to be greater at lower welding speeds — Fig. 4.

Gas Shield

Although helium gas shielding is typically employed during laser welding due to its lower ionization potential and, hence, reduced tendency to form plasma, the low density of helium makes it less suitable for welding in the flat position. Bead-on-plate trials conducted to determine the influence of shielding gas composition revealed that up to 50% argon could be added to the shielding gas stream without substantially altering the depth and width of the LAGMA weld pool (Table 3). Additions of oxygen to the shielding gas were attempted to promote spray transfer and reduce the possibility of damage to the laser focusing optics due to spatter. The addition of 4.5% oxygen to the shielding gas produced spray

Table 4 — Effects of V-Groove Angle on GMAW and LAGMAW Depth of Penetration

Groove Angle	GMAW Depth (mm)	LAGMAW Depth (mm)	Increase in Depth[a] (mm)
45	9.8	12.8	3.0
60	10.4	13.3	2.9
90	9.0	13.5	4.5

(a) LAGMAW Depth — GMAW Depth.

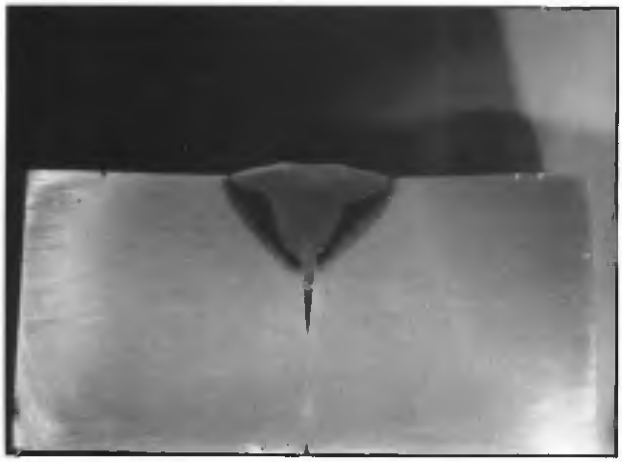

Fig. 7 — Incomplete penetration in V-groove with a 15-deg included angle. Root opening 0 mm (2.2X).

transfer conditions and far less spatter. However, the increased fluidity of the weld pool also introduced the requirement for welding using a backhand welding technique (an extremely poor bead profile was obtained during forehand welding), which in turn resulted in poorer weld penetration. Thus, the best penetration with LAGMAW was achieved with forehand welding procedures and an inert gas shield.

Heat Input

The effect of total heat input on weld penetration for the LAGMAW, GMAW and laser processes is shown in Fig. 5. It is, of course, difficult to make comparisons between different processes on the basis of total (rather than net or absorbed) heat input because of differences in both heat transfer efficiency and heat source intensity. A recent estimate of energy absorption efficiency for the laser process, in the keyhole mode relevant to the current discussion, and incorporating absorption effects in the plasma is 0.5 (Ref. 6), while the efficiency for GMAW is estimated to be 0.75 (Ref. 7). The focused laser source had, based on the 5-kW laser power and 1-mm beam size used, an intensity of more than 5×10^9 W/m^2. This is more intense than a GMAW source, which is unlikely to exceed 5×10^8 W/m^2 (Ref. 8). This higher intensity for the laser source would translate into a higher efficiency of melting by the absorbed energy in the laser case. The efficiency and intensity of the hybrid LAGMAW process is unknown, although as mentioned in the introduction, it is felt that focusing the arc along the laser beam increases intensity over the GMAW limit. What Fig. 5 does show is that, for the 5-kW laser, the weldments produced using the LAGMAW process required less total heat input to produce a given weld penetration than either the GMAW or laser welding process alone. For example, 8-mm-deep, bead-on-plate LAGMA welds could be produced using processing parameters producing a theoretical heat input of approximately 1.0 kJ/mm. Similar GMA weld penetration would require welding parameters producing approximately 50% higher total heat input. Laser welding alone using 5700 W of power and a heat input of 1.35 kJ/mm was able to produce a maximum penetration of only 7.5 mm. Figure 6 shows there is considerable scatter in heat-affected zone width for both the LAGMAW and the GMAW processes over the range of heat inputs investigated. Thus, comparisons of heat-affected zone width as a function of penetration or heat input for the various processes cannot be made at this time.

Table 5 — Effect of Heat Input on the Microhardness of Bead-on-Plate Laser-Assisted Gas Metal Arc Welds Made with a 50% He-50% Ar Gas and a Laser Power of 5.1 kW

Arc Voltage (V)	Arc Current (A)	Welding Speed (mm/s)	Preheat °C	Heat Input (kJ/mm)	Weld Metal Hardness (HV 300 g)	Coarse-Grained HAZ Hardness (HV 300 g)
30	420	12.7	20	1.39	391	424
30	395	8.5	20	2.00	379	432
30	400	12.7	93	1.35	391	416

Table 6 — LAGMAW Procedure for Welding 25-mm-Thick HY-80 Plate for Toughness Tests

Processing Parameter	
Shielding gas composition	50%He–50% Ar
Welding speed	10.6 mm/s
Welding direction	Forehand
Laser output power	5000 W
Electrode polarity	DC electrode positive
Electrode type	Lincoln LA 100, 1.6-mm diameter
Arc current	390–440 A
Arc voltage	28 V
Heat input	1.6 kJ/mm
Groove preparation	Double 45-deg V, 9.5 mm deep, no root opening
Number of passes	4
Preheat temperature	93°C minimum
Interpass temperature	93–149°C
Torch position:	
C	15 mm
θ	50 deg
X	0.0 mm
Z	Focal point 4.4 mm below groove bottom

Joint Configuration for Butt-Joint Welds

Preliminary processing trials utilizing bead-on-plate techniques clearly demonstrated deeper penetration could be achieved by adding laser energy to the GMAW process while producing lower heat input to the workpiece. However, the resulting weldments generally did not consistently display sufficient penetration (greater than 12.7 mm) to allow for the development of a two-pass welding process utilizing a butt-joint configuration. In general, the LAGMAW bead-on-plate trials produced welds up to approximately 10 mm deep.

Additional trials to determine the effect of weld groove design were performed using 8-mm-deep V-grooves machined to 45-, 60- and 90-deg angles. These trials revealed greater depth of penetration could be achieved in wider grooves (Table 4). Narrower V-grooves (from 7 to 30 deg) tended to produce inconsistent penetration (and incomplete penetration for the narrowest grooves), as shown in Fig. 7. The introduction of a gap at the root of the narrower V-grooves improved penetration, but required an additional pass to fill the extra groove volume. A 45-deg V-groove with no root opening was considered to be the optimum design

for LAGMAW of thick steel plate, since wider grooves would require more welding passes for complete filling of the joint.

Effect of Heat Input and Shielding Gas Oxygen Content on Microstructure

To simplify the approach to the large number of variables that might affect microstructure, only heat input and weld metal oxygen content were considered in detail. Other independently adjustable parameters were set to the values determined to give best penetration. Microstructural development was examined in three steps. In step one, we examined the effect of heat input on the microstructures of bead-on-plate weldments made with a 50% He-50% Ar shielding gas, LA-100 wire and HY-80 plate. The results of some of these experiments are shown in Table 5. The hardness values in both the weld metal and coarse-grained heat-affected zones are consistent with the hardnesses expected from untempered martensite with carbon contents typical of the two zones. Metallography revealed the microstructure in the coarse-grained heat-affected zone consisted of martensite, as did the fine-grained heat-affected zone. The weld metal itself seemed to be predominately martensitic. Little of the acicular ferrite associated with high toughness weldments was observed. The microstructures of all the bead-on-plate weldments were similar to those of the multipass weldment shown in Fig. 8, which was produced with the parameters shown in Table 6.

In step two, the effect of heat input on the microstructure of single- and double-pass weldments was examined. The weldments were produced with a 47.7% He, 47.7% Ar, 4.6% O_2 shielding gas; a 45-deg, 7.1-mm-deep V-groove preparation; in HY-80 plate and with LA-100 welding wire. The purpose of this step was to see if oxygen additions would allow an acicular ferrite weld metal microstructure to be produced. The results are summarized in Table 7. It was realized that dilution of the weld metal with manganese-lean base plate would affect microstructural development. Thus, dilution was estimated using a roller planimeter to make the measurements described by, for example, Ref. 9. As shown in Table 7, dilutions of 30 to 60% were estimated, assuming no loss of al-

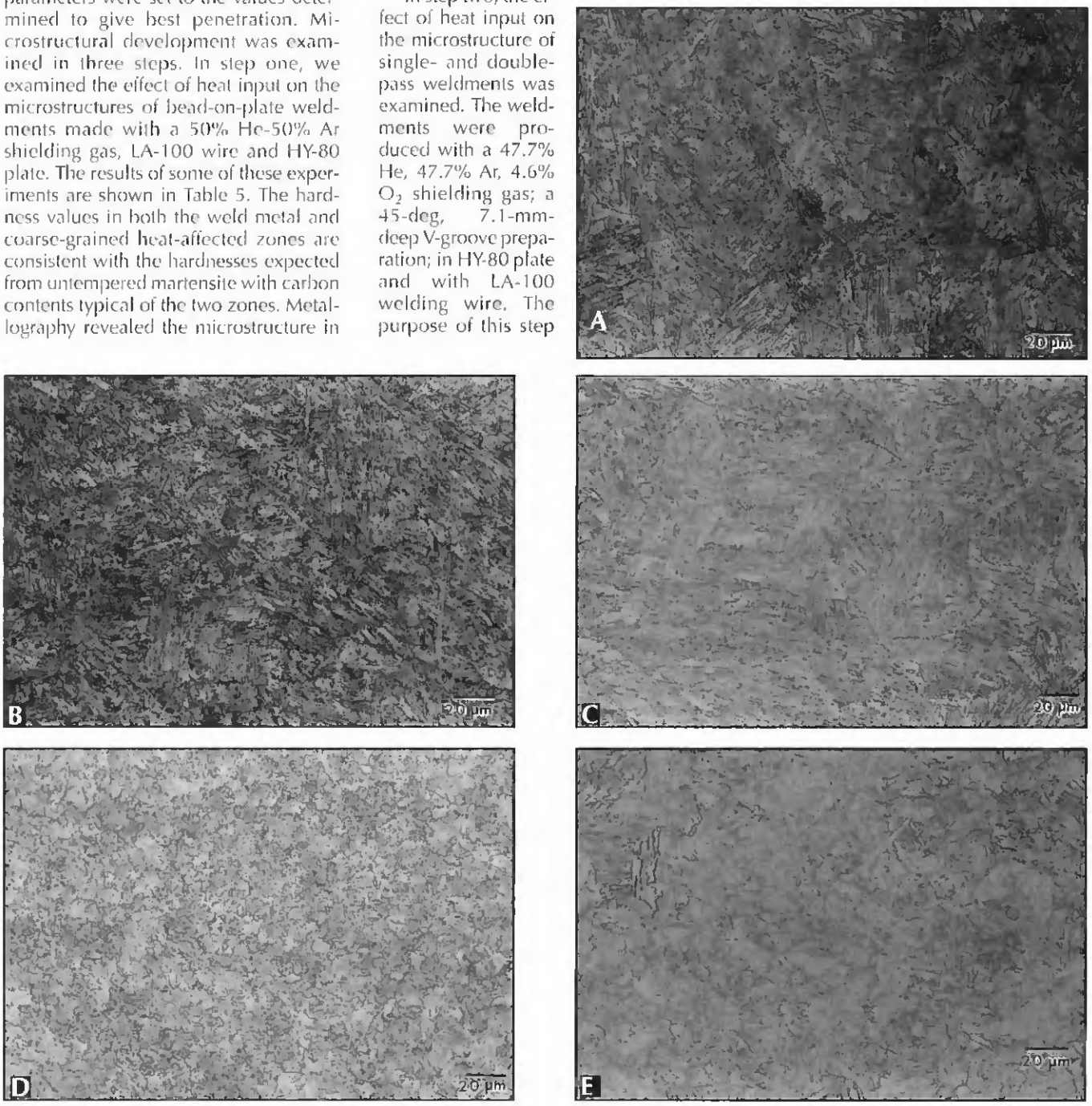

Fig. 8 — Typical microstructures in four-pass LAGMA weld in HY-80 steel (440X). A — Weld metal; B — weld metal heat-affected zone; C — large-grained heat-affected zone immediately adjacent to the weld interface; D — small-grained heat-affected zone; E — base metal.

Table 7 — Hardness and Dilution in HY-80 Welded with 1.6-mm LA-100 Welding Wire and an Atmosphere Containing 4.6% Oxygen

Heat Input (kJ/mm) pass 1/pass 2	Preheat/ Interpass (°C)	Dilution (% Filler)	Estimated Composition C	Estimated Composition Mn	Coarse-Grained HAZ (VHN) Ave ± Std. Dev.	Weld Metal hardness (VHN) Pass 1 Ave ± Std. Dev.	Weld Metal hardness (VHN) Pass 2
2.17	98	29	0.11	0.66	421.8 ± 19.6	330.1 ± 5.4	—
2.08	97	29	0.11	0.66	425.8 ± 8.2	305.5 ± 7.4	—
2.19	155	33	0.11	0.71	407.2 ± 14.9	301.6 ± 8.5	—
2.12	200	33	0.11	0.71	392.8 ± 21.0	282.0 ± 7.3	—
1.08/1.06	97/121	58	0.09	1.02	411.4 ± 6.6	355.8 ± 18.7	341.8 ± 14.0
1.09/1.01	210/208	50	0.09	0.92	412.4 ± 12.6	288.4 ± 4.0	291.6 ± 11.7
1.06/0.99	266/264	48	0.10	0.89	396.8 ± 15.0	272.0 ± 5.1	280.2 ± 6.4

Notes: All welds produced using backhand welding technique.
Torch angle = 30 deg (to the horizontal).
Laser beam focal point position = 4.4 mm below groove bottom.
Shielding gas composition = 40 ft³/h Ar + 40 ft³/h He + 3.8 ft³/h O_2 (47.7% Ar + 47.7% He + 4.6% O_2).
Laser output power = 4650–4800 W.
Welding Speed = 7.6 mm/s (single pass), 15.2 mm/s (double pass).
Welding current = 370–430 A.
Welding voltage = 27–28 V.

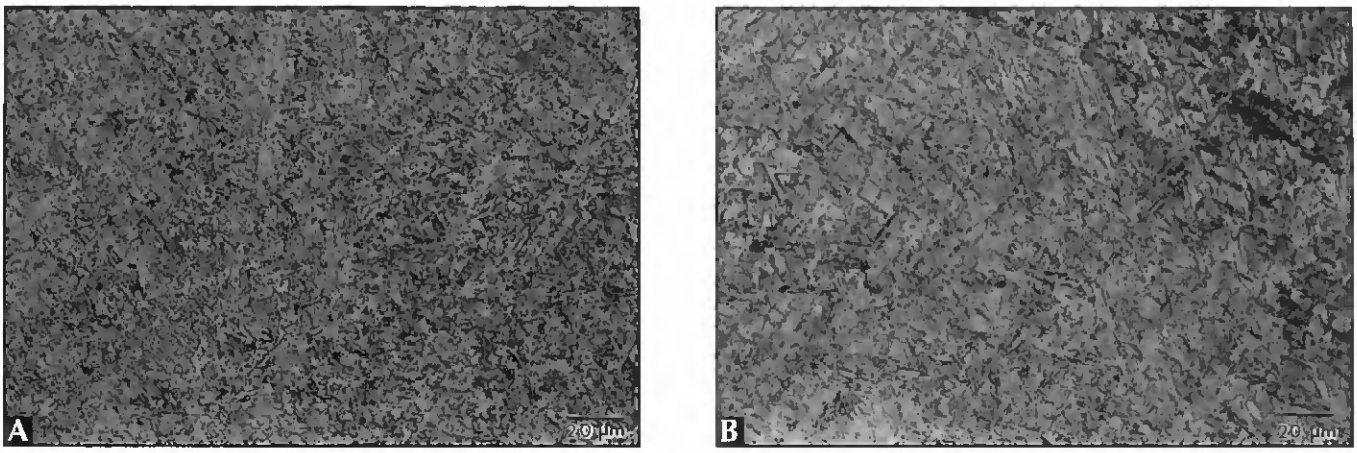

Fig. 9 — Weld metal microstructures obtained during welding of HY-80 steel with an LA-100 wire and shielding gas containing A — 1% oxygen addition; B — 3% oxygen addition.

loying elements. These estimated dilutions were in agreement with X-ray microanalysis results in a number of locations. Microstructural analysis revealed little or no acicular ferrite in any of the step two weldments. Instead, using the terminology adopted by IIW (Ref. 10), the weld metal microstructures contained mainly ferrite with aligned and nonaligned second phase. Primary ferrite was also observed in the single-pass weldments. The two-pass weld preheated to the lowest temperature consisted primarily of martensite with some ferrite with aligned second phase and grain boundary ferrite. For each of these weldments, except where a preheat above 200°C was used, the microstructure of the coarse-grained heat-affected zone was predominately martensitic. Hardnesses observed were consistent with this. Based on previous work, it is likely the volume fraction of martensite in all heat-affected zones was reduced for preheat and interpass temperatures above 150°C (Ref. 11).

In step three, the effect of oxygen level in the shielding gas was examined at a constant heat input of 1.6 kJ/mm to see if an acicular ferrite structure could be produced. Again, 45-deg V-grooves machined into HY-80 plate and LA-100 welding wire were used. Parameters were similar to those used in step two, except that, in this case, additions of 0, 1 and 3% oxygen were made to the base 50% He-50% Ar shielding gas. Microstructural analysis revealed largely martensitic weld metal microstructures were produced in the absence of oxygen — Fig. 8A. Some Widmanstätten α was found to nucleate on nonmetallic inclusions in the weldment produced using a shielding gas containing oxygen — Fig. 9A. Adding 3% oxygen to the gas mix produced ferrite with aligned and nonaligned second phase, grain boundary ferrite and possibly a very minor amount of fine acicular ferrite — Fig. 9B. However, none of the conditions in step three produced a microstructure containing predominately acicular ferrite.

As mentioned earlier, increasing the oxygen content of the shielding gas produced weld metal structures containing greater volume fractions of ferritic constituents (Fig. 9) as compared to the largely martensitic microstructure produced using helium/argon shielding gas — Fig. 8. Even though increased oxygen favors tough acicular ferrite structures, little acicular ferrite was observed. It was believed dilution of the electrode metal with HY-80 plate produced a weld metal chemistry that did not favor acicular ferrite formation. According to Ref. 12, the dilutions reported in Table 7 are probably sufficiently high (Mn sufficiently low) that acicular ferrite formation would be suppressed. This is supported by the observation that acicular ferrite was produced in laser-assisted gas metal arc

Table 8 — Impact Test Results

Notch Location	Test Temperature (°C)	Dynamic Tear Energy (J)	Shear Lip (mm)	Weld Zones on Fracture Surface[a]
Weld Metal	–45	404	2.54	70% WM, 30% RHWM
Weld Metal	–45	129	1.45	75% WM, 25% RHWM
Weld Metal	–30	601	4.43	80% WM, 20% RHWM
Weld Metal	–30	1256	4.79	50% WM, 20% RHWM, 25% BM
Weld Metal	–15	511	2.73	80% WM, 20% RHWM
Weld Metal	–15	1547	4.38	80% WM, rest BM and HAZ
Weld Metal	0	962	4.51	80% WM, 20% RHWM
Weld Metal	15	1958	5.31	70% WM, rest BM
Heat-Affected Zone	–45	1998	5.28	60% BM, rest WM or HAZ
Heat-Affected Zone	–30	1800	5.2	50% BM, rest HAZ
Heat-Affected Zone	0	1956	5.74	50% BM, most of the rest WM
Heat-Affected Zone	15	2883	6.16	BM

(a) BM—Base metal; WM—Weld metal; RHWM—Reheated weld metal; HAZ—Heat-affected zone.

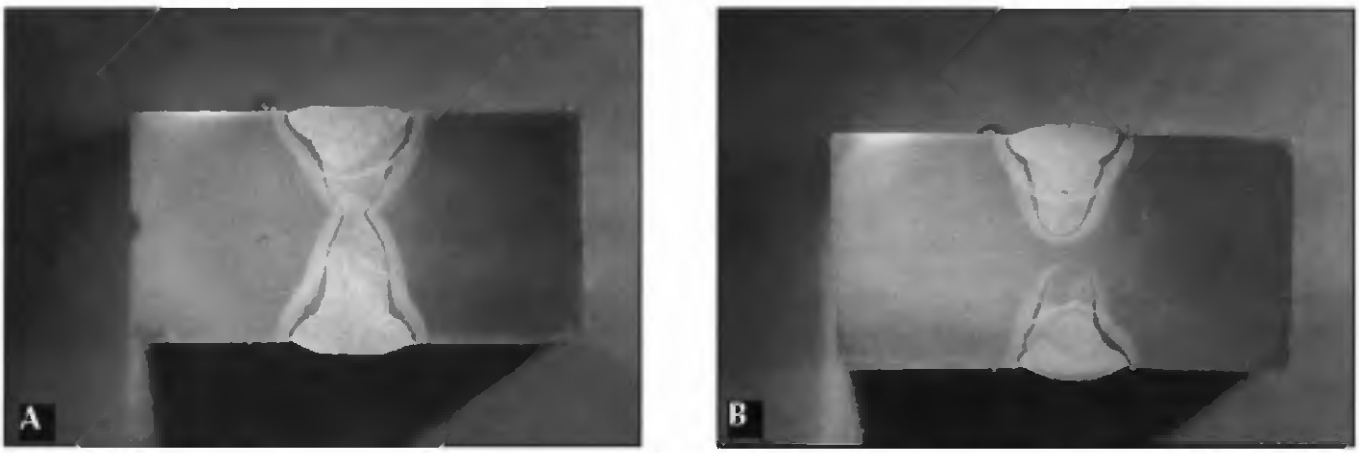

Fig. 10 — Macrographs (1.5X). A — Four-pass LAGMA weld for joining 25-mm-thick steel plate; B — equivalent GMA weld showing incomplete penetration.

weldments produced using the same wire but a 300-W base plate, which has a higher manganese level. There may also be other compositional factors that caused the formation of acicular ferrite to be suppressed (Ref. 13).

To aid in the selection of variables for the preparation of specimens for toughness testing, preliminary toughness tests were done on specimens made in step 3. These experiments showed the weldments prepared without oxygen additions to the shielding gas had the highest toughness.

Preparation and Characterization of Coupons Used for Dynamic Tear and Explosion Bulge Testing

Although adequate penetration could generally be achieved using a two-pass welding procedure in 45-deg V-grooves, occasional incomplete penetration was observed. For this reason, a four-pass welding procedure was selected for the production of materials for toughness evaluation to ensure full penetration through the root of the groove preparation. A cross section through the resulting welded joint in 25-mm-thick HY-80 steel plate displayed good penetration — Fig. 10A. For comparison, a four-pass weldment produced using essentially the same GMAW parameters revealed an incomplete penetration — Fig. 10B. The welding parameters used to produce the LAGMA weldments are listed in Table 6. Note that a heat input of 1.6 kJ/mm and an argon/helium atmosphere without oxygen addition were used.

The microstructure of the four-pass LAGMA weld consisted of martensite/bainite and tempered martensite within the weld and coarse-grained heat-affected zones. A fine-grained structure existed in the heat-affected zone located further from the weld. Typical microstructures are shown in Fig. 8. The hardest microstructure was the coarse-grained heat-affected zone (401 HV), and the softest was the fine-grained heat-affected zone (304 HV). The weld metal displayed an intermediate hardness (326–362 HV).

Evaluation of Toughness by Dynamic Tear Testing

A toughness transition curve for the weldment was produced using the ASTM E604 dynamic tear test (Ref. 14) and 25-mm-thick specimens. In an effort to learn about the heat-affected and weld metal zones, notches were machined and pressed into the heat-affected zone of some specimens, while on others the notches were machined and pressed into the weld metal. For both types of specimen, dynamic tear energies and shear lip sizes were measured. Dynamic tear energy is used as a measure of resistance to rapid progressive fracture. Although the results are only indirectly relatable to stress analysis (Ref. 15), energies obtained are a good measure of the fracture toughness. As well, there is a large body of meaningful published data on dynamic tear energies and shear lip sizes for HY-80 weldments and other materials of high toughness (Refs. 16–18).

Following the technique outlined in Ref. 17, shear lip measurements were

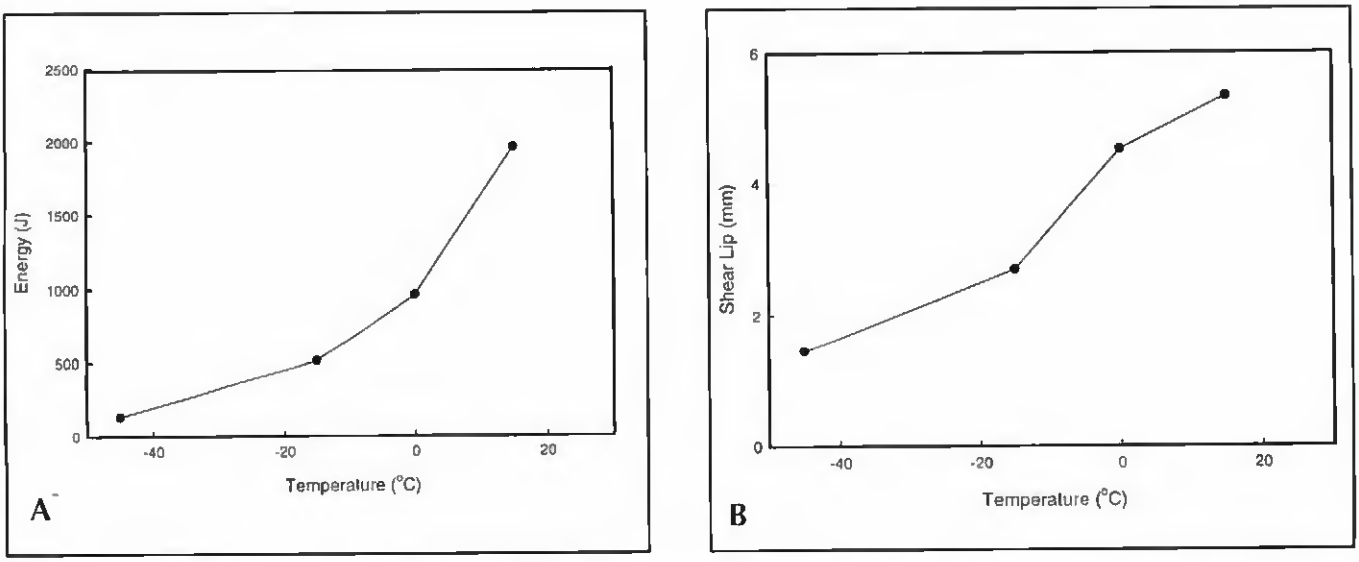

Fig. 11 — A — Weld metal dynamic tear energy; B — shear lip size. Both are a function of temperature for the laser-assisted gas metal arc weld.

made by measuring the distance between the two shear lips, subtracting that from the original specimen width and dividing by two to obtain an average shear lip width. Such shear lip width measurements provide an alternative to percent shear (Ref. 14), which has been shown to directly correlate with the dynamic tear energy. Shear lip measurements can be used on their own to obtain transition behavior or as a way to check that measured dynamic tear energies are reasonable.

One difficulty conducting tearing resistance-type tests (as opposed to fracture initiation tests) is that the inhomogeneous nature of weldments makes it unclear what is contributing to the energy of tearing. To assess what microstructures the dynamic tear energies actually referred to, following the method described in Ref. 19, half of each broken dynamic tear specimen was sectioned perpendicular to the fracture surface along a line parallel to the notch tip. Sections taken 4 mm from the notch tip and 12 mm from the edge of the specimen opposite the notch were etched, and the portion of the line across the fracture surface where weld metal, reheated weld metal, heat-affected zone material or base material was estimated. By averaging these two values, an estimate of the fraction of each type of material on the fracture surface was made.

The results of the dynamic tear tests are show in Table 8 and Fig. 11. Also shown in Table 8 is the fraction of each type of material on the fracture surface. It is clear none of the specimens intended to test heat-affected zone properties actually did so. In all cases, cracks ran into the base plate. However, in the weld metal specimens, the crack stayed in the weld metal for the most part. Thus, the weld metal tests adequately tested weld-metal tearing resistance. One concern with the weld metal specimens is the occasional observation of welding discontinuities (gas porosity) on the fracture surface. It is felt that such discontinuities probably do not have a dominant effect on measured toughness. The reason for these discontinuities is unclear. Gas shielding parameters, speed and low manganese level may all have played a role.

Explosion Bulge Testing

The DREA monoblast, underwater explosion bulge procedure (Refs. 20–22), a modified version of the American Military Standard procedure (Ref. 23), was employed to evaluate a laser-assisted gas metal arc welded 61-x 61-x 2.54-cm panel. In this procedure, a chilled, full-scale test piece is placed on an anvil that has a 38-cm circular hole in the center. An explosive charge of appropriate weight is suspended above the test piece. The entire assembly is then submerged in water and the charge detonated once the test piece attains the testing temperature of –5°C. The explosive energy is transferred through the water and deforms the center of the test piece into the anvil opening, thus generating high biaxial plastic strain throughout the center portion of the weldment system. In the DREA procedure, the charge weight is selected to achieve the required pass/fail degree of plate thinning in a single loading event. For HY-80 plates and weldments, the DREA recommended degree of thinning in the bulge apex adjacent to the weld metal is 16%. This is in keeping with the American Military Standard for HY-80 steel plates (Ref. 24) but is more demanding than the corresponding American Military Standard for HY-80 weldments (Ref. 25). To attain 16% thinning in 2.54-cm-thick HY-80 weldments, the required charge weight is approximately 5.5 kg. To satisfactorily pass these evaluations, the test panels must achieve the desired degree of thinning without expelling fragments or developing a through-thickness crack or developing a surface crack extending into the hold-down region.

Following the explosive deformation of the laser-assisted gas metal arc weldment, no visible cracking or ejected fragments were observed. Ultrasonic through-thickness measurement of the material adjacent to the weld in the bulge apex was not possible due to the formation of subsurface delaminations or defects. Measurements made at locations within the bulge apex, but several centimeters from the prescribed measurement location, indicated a plate thinning of 13%. Unfortunately it was not possible to subsequently section the panel and examine the generated defects or make additional thinning measurements. Given the level of thinning would be higher at the prescribed measurement location and the explosive configuration employed was sufficient to generate the required thinning, it is reasonable to conclude this panel satisfactorily passed the evaluation.

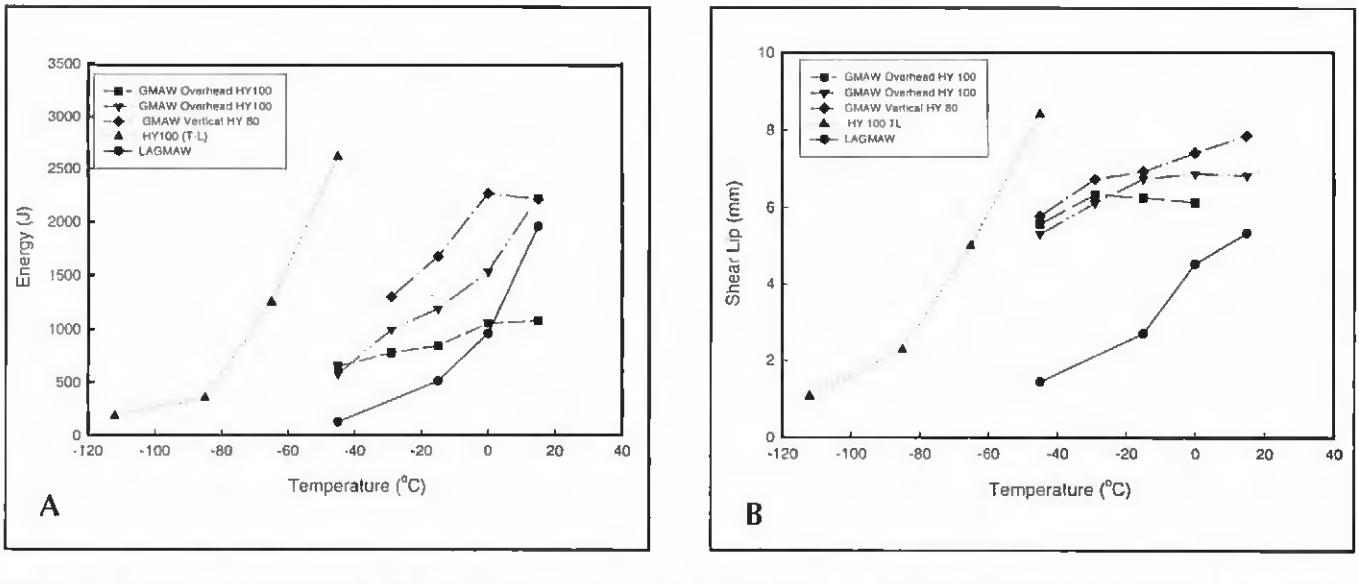

Fig. 12 — A — Lower bound weld metal dynamic tear energy; B — shear lip size. Both are as a function of temperature for the laser-assisted gas metal arc weld and several gas metal arc welds.

Discussion

The results above show, provided operating parameters are correctly chosen, laser-assisted gas metal arc welding can improve penetration and welding speed and reduce the amount of consumable material required relative to arc welding processes at the same heat input. For HY-80, the use of traditional arc welding consumables may be limited by the formation of nonoptimum weld metal microstructures caused by excessive dilution of the weld metal. A customized consumable containing higher manganese content may be required to obtain the desired acicular ferrite weld microstructure. This might also have an effect on porosity, though a systematic study is required to understand the variables that affect porosity formation. The same dilution effects can also be expected in other deep penetration welding processes in which HY-80 and similar consumables are used.

Understanding the significance of dynamic tear measurements requires comments on the toughness levels required, the relationships between more traditional 16-mm specimens and full-plate-thickness, 25-mm specimens, and comparison with data of other welding methods. For the 16-mm specimen and a variety of 100 and 120 S-1 and S-2 consumables, Ref. 25 states, depending on consumable type, dynamic tear energies of above 406 to 524 J (300 to 400 ft-lb) constituted satisfactory toughness levels at –29°C (–20°F) and energies above 610 to 780 J (450 to 575 ft-lb) constituted satisfactory toughness levels at –1°C (30°F). More recently, it has been suggested, by workers from a number of countries, that 690 J at –29°C would be a more realistic minimum DT toughness for the 16-mm specimen. The goal of welding research, however, is to acquire toughness levels for weldments on the order of the toughness level for HY-80 steel (T-L orientation). This would place the target level in the 900–1200 J level. Comparing the 16- and 25-mm specimens, toughness level requirements for 25-mm specimens are about the same for midpoint transition and lower, but would be 25% higher for upper shelf (Ref. 17).

There is a variety of relevant data on the toughness of welds tested using 16-mm specimens and a –29°C testing temperature. For a variety of gas metal arc welds in HY-80, using 16-mm specimens and a –29°C testing temperature, toughnesses from values of 600 to 1200 J have been reported. Submerged arc welding gave values, probably in the transition zone of the curve, of 544 J for a 2-kJ/mm heat input and 237 J for a 4-kJ/mm heat input. Shielded metal arc welds produced using E12018 M2 electrodes gave values of 267 to 407 J (Refs. 15, 16, 26).

For purposes of comparing the transition curve shown in Fig. 11, weld metal toughness data from Ref. 18, which shows transition curves produced using 25-mm DT specimens for pulsed gas metal arc welds produced using TIME gas and 100 S1 wire, are shown in Fig. 12. Also shown are data from the same source (Ref. 18) on the toughness of conventional and pulsed gas metal arc welds in HY-100 using 120 S1 wire.

For a test temperature of –30°C, the 25-mm, laser-assisted gas metal arc weld specimens tested in this work gave a dynamic tear energy of 601 J for a specimen in which the crack was entirely in the weld metal. However, from the lower bound limit of the transition curve for the LAGMA weldment (Fig. 10), the –30°C limit is 250 J. For engineering purposes, the lower bound value is relevant. On this level the LAGMA weldments are clearly inferior to the gas metal arc weldments shown in Fig. 12. Using the guidelines mentioned above to compare energies from 25-mm and 16-mm specimens, the lower bound results are comparable, or somewhat inferior, to high-quality application of other types of welding to 1-in.-thick HY-80. The suggested 690 J at –29°C requirement was not achieved.

From a research perspective, there is reason for optimism. Even though metallography showed cracks were predominately running in the weld metal, these results show the largest amount of scatter in dynamic tear energy of any weldment we have tested. The high level of scatter in the LAGMA weldments and the high DT energies measured at –30°C suggest better results could be achieved. The DT tests were all done on plates welded with a helium-argon gas mix. The nominal heat input, neglecting efficiency considerations, was 1.6 kJ/mm. Taking into account efficiencies, which have not been measured for the LAGMAW process, the actual heat inputs are probably somewhat lower. For gas metal arc welding, our experience has been that weld metal

toughnesses like those shown in Fig. 12 are normally achieved with heat inputs slightly less than 1 kJ/mm. However, good results have been achieved with heat inputs up to 2.5 kJ/mm. We believe in the LAGMAW case, the heat inputs and gas shield are not likely the main source of the toughness variability. A logical next step in the work would be the development or selection of a consumable alloy that could tolerate the 50% per pass dilution associated with the LAGMAW process. Following on from this, parameters would need to be adjusted to reduce the defect level. Finally, the effects of heat input and oxygen level should be reexamined. It is felt that optimization of heat input could give improvements in toughness.

Particularly for narrow-groove welds, but probably for all welds, these results show the need to ensure that toughnesses quoted actually refer to the weld metal, rather than some combination of base metal and weld metal. This was not done for the weldments to which these results were compared. It is interesting that for the laser-assisted gas metal arc weld, the shear lip results do not mirror the dynamic tear energies in the way the other weldments shown in Fig. 12 do. This may be a result of the presence of defects impeding the formation of shear lips. Alternatively, it may be that the higher dilution of the inner passes of the weldment gave them intrinsically lower toughness, and thus limited shear lip formation in this region. These are questions that could be considered in a future study with a different consumable. In general, the relationship between fracture surface information and dynamic tear energy for narrow groove weldments needs further consideration.

This work has practical implications for laser welding facilities equipped with relatively low power CO_2 and YAG lasers that wish to weld thicker materials. These results show this can be done in a way that retains the advantages of laser welding.

Conclusions

Laser-assisted gas metal arc welding using Lincoln LA-100 wire on 25-mm HY-80 plate with a four-pass technique produced a predominately martensitic weld metal microstructure. An acicular ferrite weld metal microstructure could not be produced for any set of processing conditions investigated. This is believed to be a result of high levels of dilution. The toughness of the laser-assisted gas metal arc welds was below acceptable levels based on lower bound values. Thus, at least with the consumable and conditions investigated in this work, laser-assisted gas metal arc welding is not an acceptable technique for welding of HY-80 plate at present. However, the considerable scatter in toughness results and the high upper bound toughness values suggest this is a promising technique, perhaps worthy of additional work, for example in the area of developing an electrode chemistry that would tolerate high levels of dilution and allow toughness to be improved.

References

1. Magee, K., Merchant, V. F., and Hyatt, C. V. 1991. Laser-assisted gas metal arc weld characteristics. *Laser Materials Processing*, Vol. 71, pp. 382–399.

2. Matsuda, J., Utsumi, A., Katsumura, M., Hamasaki, M., and Nagata, S. 1988. TIG or MIG arc augmented laser welding of thick mild steel plate. *Joining and Materials* 1(1): 31–34.

3. Eboo, M., Steen, W. M., and Clarke, J. Arc Augmented Laser Welding, 4th Int. Conf. of Advances in Welding Process, Paper 17, May, 1978, Harrogate, U.K.

4. Diebold, T. P., and Albright, C. E. 1985. Laser-GTA welding of aluminum alloy 5052. 65th AWS Annual Meeting, Dallas, Tex.

5. Magee, K. H. 1993. An experimental study of laser-assisted arc welding. *DREA CR/93/430*, Defence Research Establishment Atlantic, Dartmouth, Nova Scotia, Canada.

6. Duley, W. W. 1999. *Laser Welding*, New York, N.Y.: John Wiley and Sons, Inc., p. 80.

7. Easterling, K. E. 1983. *Introduction to the Physical Metallurgy of Welding*, London, England: Butterworths and Co., p. 18.

8. Devletian, J. H., and Wood, W. E. 1983. Principles of joining metallurgy, *Metals Handbook*, Vol. 6, 9th Ed., Welding Brazing and Soldering, p. 32.

9. Linnert, G. E. 1965. *Welding Metallurgy*, Miami, Fla: American Welding Society, pp. 436–439.

10. Pargeter, R. J., Harrison, P. L., and Kelly, P. O. 1985. *Compendium of Weld Metal Microstructures and Properties (Submerged Arc Welds in Ferritic Steel)*. Published for the International Institute of Welding by TWI, Cambridge, U.K.

11. Gianetto, J., Bowker, J. T., and Letts, M. W. 1993. Evaluation of heat-affected zone microstructure/mechanical properties of HY100 grade steel. *DREA CR/93/451*, Defence Research Establishment Atlantic, Dartmouth, Nova Scotia, Canada.

12. Grong, O., and Matlock, D. K. 1986. *International Metals Review*, Vol. 31, pp. 37–48.

13. Abson, D. J., and Pargeter, R. J. 1986. *International Metals Review*, Vol. 31, pp. 141–194.

14. *Standard Test Method for Dynamic Tear Testing of Metallic Materials*. ASTM E604-83. 1987. Annual Book of ASTM Standards. Philadelphia, Pa: ASTM, pp 829–840.

15. Ravichandran, K. S., and Vasudevan, A. K. 1966. Dynamic fracture testing, Appendix 2, *Fracture Resistance of Structural Alloys*, Vol. 19, *ASM Handbook, Fatigue and Fracture*. Materials Park, Ohio: ASM International, pp. 403–409.

16. Matthews, J. R., Porter, J. F., Church, J., and Macecek, M. 1991. An evaluation of TIME welding of HY80 plate. *Welding Journal* 70(2): 35–41.

17. Matthews, J. R. 1996. On the relationship between shear lip, shear index and energy in dynamic tear specimens. *Engineering Fracture Mechanics* 54(1): 11–23.

18. Matthews, J. R. 1997. Prediction of ductile behavior in welded structures, (transition behaviour, shear lip, notch acuity, and specimen size). *Recent Advances in Fracture*, R. K. Mahidhara, A. B. Geltmacher, P. Matic and K. Sadananda, eds. Warrendale, Pa: TMS, pp. 159–170.

19. Gianetto, J. A., Tyson, W. R., Matthews, J. R., Bowker, J. T., and Braid, J. E. M. 1996. Microstructures and properties of high strength submerged arc weldments. *International Conference on Advances in Welding Technology*, Columbus, Ohio.

20. Porter, J. F., and Matthews, J. R. 1991. The role of explosion bulge trials in submarine materials research at DREA. *TTCP Workshop on Methods for Approval of Materials for Use in Submarine Hulls*, DTRC, Annapolis, Md.

21. Porter, J. F., and Ahmad, J. 1990. *Proceedings of the 61st Shock and Vibration Symposium, Jet Propulsion Laboratory*, Vol. IV Pasadena, Calif.: California Institute of Technology, pp. 101–111.

22. Porter, J. F., Morehouse, D. O., and Gorveatte, G. 1993. Monoblast explosion bulge evaluation of HYW700QT submarine pressure hull steel. *Abstracts and Summaries of the CF/CRAD Meeting on Naval Applications of Materials Technology*, Halifax, Nova Scotia, Canada.

23. *Standard Procedures for Explosion Testing Ferrous and Non Ferrous Metallic Materials and Weldments*, Mil-STD-2149(SH). 1983. Washington, D.C.: Dept of the Navy, Naval Sea Systems Command.

24. *Military Specification, Steel Plate, Alloy, Structural, High Yield Steel (HY80 and HY100)*, MIL-S-16216J(SH). Washington, D.C.: Dept of the Navy, Naval Sea Systems Command.

25. *Military Specifications, Electrodes and Rods Welding, Bare, Solid, or Alloyed Cored, Low Alloy Steel*, Mil-E-23765/2D(SH). 1987. Washington, D.C.: Dept of the Navy, Naval Sea Systems Command.

26. Matthews, J. R. 1991. *Engineering Fracture Mechanics* 39(1): 131–140.